This document is the accepted manuscript version of the following article:
Sternitzke, V., Kaegi, R., Audinot, J. -N., Lewin, E., Hering, J. G., & Johnson, C. A. (2012). Uptake of fluoride from aqueous solution on nano-sized hydroxyapatite: examination of a fluoridated surface layer. Environmental Science and Technology, 46(2), 802-809. http://doi.org/10.1021/es202750t

The Uptake of Fluoride from Aqueous Solution on Nano-Sized Hydroxyapatite: Examination of a Fluoridated Surface Layer

Vanessa Sternitzke[*†‡], *Ralf Kaegi*[†], *Jean-Nicolas Audinot*[□], *Erik Lewin*[¦], *Janet G. Hering*[†‡§] *and C. Annette Johnson*[†]

[†] Eawag, Swiss Federal Institute of Aquatic Science and Technology, Duebendorf, Switzerland

[‡] Institute of Biogeochemistry and Pollutant Dynamics, Department of Environmental Sciences, Swiss Federal Institute of Technology Zurich-ETH, Zurich, Switzerland

[□] Centre de Recherche Public Gabriel Lippmann, Department of Sciences and Analysis of Materials, Belvaux, Luxembourg

[¦] Empa, Swiss Federal Laboratories for Materials Science and Technology, Laboratory of Nanoscale Materials Science, Duebendorf, Switzerland

[§] School of Architecture Civil and Environmental Engineering, École Polytechnique Féderale de Lausanne-EPFL, Lausanne, Switzerland

* Corresponding author phone: +41 58 765 5370; fax: +41 58 765 5210; e-mail: vanessa.sternitzke@eawag.ch

ABSTRACT

Hydroxyapatite ($Ca_{10}(PO_4)_6(OH)_2$, HAP), both as a synthetic material and as a constituent of bone char, can serve as an effective and relatively inexpensive filter material for fluoride (F^-) removal from drinking water in low-income countries. Fluoride uptake on HAP can occur through different mechanisms, which are, in principle, influenced by solution composition. Suspensions of HAP (2 g L^{-1}) were equilibrated under controlled pH conditions (pH 6.5, 7.3, 9.5) at 25 °C for 28 d after the addition of different F^- concentrations (0.5 - 7.0 mM). The reacted HAP solids were examined with Transmission Electron Microscopy (TEM), Fourier Transform Infrared Spectroscopy (FTIR), X-ray Photoelectron Spectroscopy (XPS) and Nano Secondary Ion Mass Spectroscopy (NanoSIMS). Fluoride uptake on HAP was dependent on pH, with the highest capacity at pH 6.5; the lowest uptake was found at pH 9.5. Under all experimental conditions, the thermodynamically stable mineral phase was fluorapatite, ($Ca_{10}(PO_4)_6F_2$, FAP). Fluoride uptake capacity was quantified on the basis of FTIR and XPS analysis, which was consistent with F^- uptake from solution. The results of XPS and NanoSIMS analyses indicate that a fluoridated surface layer with a thickness of several nanometers is formed on nano-sized HAP.

Introduction

The ingestion of elevated fluoride (F^-) concentrations via drinking water affects the health of several million humans worldwide, particularly in less developed countries.[1] Fluoride has a protective effect against tooth decay at low doses, but elevated uptake can cause dental and skeletal fluorosis.[1] The therapeutic dose and harmful levels are relatively close; the reported optimum value in drinking water to prevent tooth decay[2] is only 0.5 mg L^{-1} below the maximum guideline value of 1.5 mg L^{-1} recommended by the World Health Organization.[1] Elevated F^- concentrations are naturally present in some groundwater sources that are used for drinking water supply, for example in East Africa,[3,4] India,[5] China,[6] Mexico,[7] and Argentina.[8]

Both harmful and therapeutic health effects of F^- are related to its uptake by hydroxyapatite ($Ca_{10}(PO_4)_6(OH)_2$, HAP), the main constituent of bones and teeth.[9] Due to the propensity of HAP to take up F^-, the mineral, in the form of bone char or as a synthetic material, has been used in water treatment for F^- removal.[10, 11] In industrial countries, F^- removal is accomplished by more efficient but relatively expensive technologies, such as activated alumina and reverse osmosis.[12] In developing countries, bone char is still a viable option.[10, 13] The F^- uptake capacity of HAP is a key criterion for implementation as it directly affects the lifetime and cost of filter media. Fluoride removal efficiency can be influenced by HAP morphology and water composition, such as pH and potentially competing anions (e.g., chloride, sulphate, and carbonate).[14, 15] In order to predict the HAP filter performance, it is important to identify and quantify the contributions of possible mechanisms for F^- uptake on HAP: (i) adsorption on the surface, (ii) substitution into the crystal lattice, and (iii) (dissolution-) precipitation.

(i) Surface adsorption. In this mechanism, F^- forms surface complexes with reactive sites on HAP, such as ≡CaOH. The surface charge is controlled by the chemisorption and release of protons at this site, and also on ≡OPO_3H_2.[16] The high affinity of F^- for the HAP surface leads to exchange of water (at

acidic pH) or hydroxide ions (at neutral pH) at ≡CaOH sites. A comprehensive overview of the surface species distribution of FAP as function of pH is provided by Bengtsson et al.[16]

(ii) Substitution in the HAP crystal lattice. Fluoride ions sorbed onto the HAP surface can substitute for hydroxide (OH^-) within the HAP crystal structure.[17] This substitution is favored because F^-, with its smaller ionic radius (F^-: 0.133 nm, OH^-: 0.137 nm), fits better into the crystal structure of apatite yielding the more thermodynamically stable fluorapatite ($Ca_{10}(PO_4)_6F_2$, FAP).[18-20] This substitution process is independent of, and does not affect surface charge. It is kinetically controlled primarily by diffusion of fluoride from the HAP surface into the crystal. The formation of several nm thick surface layers of FAP on bulk HAP has been observed after 5 min[21] or 1 h[22] equilibration in F^- solutions and may hinder further incorporation of F^- into the bulk HAP.[23]

(iii) (Dissolution-)precipitation. HAP dissolution, particularly under acidic conditions, can result in an increase of calcium (Ca^{2+}) and (total, dissolved) phosphate (PO_4) concentrations in solution. If the solution becomes supersaturated with respect to solids such as FAP or fluorite (CaF_2), the precipitation of these phases can result in a decrease in dissolved solute concentrations. Such precipitation has been observed to occur either homogeneously in solution or heterogeneously on a pre-existing surface when fluoride is added to HAP suspensions.[24, 22, 25] Less stable intermediates such as CaF_2 may dissolve in favor of reprecipitation of the most thermodynamically stable phase, FAP.[26]

Although, many different studies have contributed to a general understanding of the reactions between F^- and HAP, they are difficult to compare because either HAP surface area was not reported,[27, 28] the pH was not controlled,[24, 11] or the equilibration times varied from minutes[29, 30] to months.[17] Furthermore, most studies were conducted at pH 4 – 7, which is relevant for dental care,[31, 25] rather than for environmental groundwater conditions (pH 5 - 9).

The aim of the present study was to determine the predominant mechanisms of F^- uptake on synthetic HAP as function of F^- concentration at environmentally-relevant pH values. A combination of microscopic and spectroscopic techniques was applied to examine the surfaces of the solid products to qualitatively and quantitatively evaluate the F^- uptake capacity on nano-sized HAP. The outcome provides an insight into surface reactions on HAP-based filter media during F^- removal from drinking water and might support optimization potentials of such filter systems.

Experimental Section

Chemicals and Materials

Powdered HAP was obtained from Budenheim GmbH, Germany. Its characterization as well as the synthesis of FAP as a solid reference sample is provided in the Supporting Information (S1-S2).

All other chemicals used were of at least "pro analysi" grade (p.a., from Merck and Fluka). Nanopure water (Barnstead NANOpure Diamond UV, resistivity > 18 MΩ-cm) was used for rinsing and solution preparations. Acid-washed (0.65 % HNO_3 followed by ≥ 3 rinses with nanopure water) polyethylene (PE) vessels were used for solution preparation and storage.

Influence of pH on the fluoride uptake capacity

Fluoride uptake capacity of HAP was determined in duplicate in open systems (atmospheric p_{CO2}) with nanopure water at 25 ± 1 °C. Suspensions (2 g HAP L^{-1}) were mixed by a suspended magnetic stirrer to avoid sample grinding. Prior to F^- uptake investigations, two experiments were conducted without pH adjustment to determine the equilibration time and equilibrium pH, in addition to solution equilibrium composition within 26 d.

For all following F^- uptake experiments, the suspension was pH controlled (6.5 ± 0.5, 7.3 ± 0.5, 9.5 ± 0.5) with 0.1 M HNO_3 and 0.1 M NaOH, using titration units (665, 725, and 842 with Metrohm software Tiamo 1.2.1) coupled to pH meters (Metrohm 691 and 713) and electrodes (Metrohm

6.0259.100 and 6.0258.010). Electrode two-point calibrations were performed at the start of each experiment by using Titrisol buffers (pH 4 and 9) and checked by measuring buffer of pH 7 (Titrisol). After equilibration for 3 d, F^- was added to HAP suspensions from a 0.5 M NaF stock solution to achieve initial dissolved concentrations of 0.5, 0.9, 2.0, 3.3, 5.0 and 7.0 mM. For F^- and elemental analysis (details in S3-S5, Supporting Information), filtered (0.2-μm nylon, PALL) samples (10 mL) were taken over 28 d, with more intensive sampling in the initial 24 h. It should be noted that potential effects from particles < 0.2 μm and therefore not retained by the filter were not investigated in detail; these could have the effect of increasing the elemental concentrations in the solutions.

Samples (20 mL) for total dissolved inorganic carbon (DIC) analysis were taken prior to the addition of F^- and at the end of the 28d-equilibration time. For cation analysis, samples were acidified with 1 % suprapure HNO_3 and stored at 4 °C until analysis. Measured elemental concentrations were corrected for the solution volume and solid loss. A 28d-equilibration period was chosen because F^- concentrations did not vary more than 5 % within the final week. The remaining solid material was collected on a 0.45-μm cellulose-nitrate filter (Sartorius), air-dried, and stored at room temperature for further analysis.

Influence of different anions on the fluoride uptake capacity at fixed pH

The effect of competing anions on F^- uptake on HAP was assessed in duplicates using the same setup as described above, at pH 7.3 and 0.5 mM initial F^-, but with a shortened equilibration time of 7 d (when 80 - 90 % of the initial F^- was taken up from solution in batches without anion addition). Chloride (Cl^-) and sulphate (SO_4^{2-}) were added from stock solutions (5.0 mM and 2.5 M NaCl, and 5.0 mM and 1.5 M Na_2SO_4, respectively) to achieve total dissolved concentrations of 0.5, 5.0 and 50 mM simultaneously with the addition of F^-.

To assess the influence of 5.0 and 50 mM HCO_3^-, the system was covered with a septum lid, and a N_2-gas mixture containing 16,100 ± 2,000 ppm CO_2 (PanGas) and a tenfold higher concentration

respectively, was bubbled directly into the suspension at a rate of approximately 0.05 - 0.10 L min^{-1}. The gas mixture, together with 0.1 M NaOH, was used for pH adjustment throughout the experiment, including a 3d-pre-equilibration. The DIC was monitored during the experiments.

Solid characterization

Transmission Electron Microscopy (TEM, Tecnai, F30ST, FEI) was performed on pure unreacted HAP and FAP, and on solids of 28d-reacted HAP from batches conducted at pH 6.5 with 7.0 mM initial F^- (highest F^- uptake from solution) and at pH 9.5 with 2.5 mM initial F^- (low F^- uptake from solution). An acceleration voltage of 300 kV was used. The microscope was operated in the scanning mode and the solids were localized using a High-Angle Annular Dark Field (HAADF) detector and analyzed with an Energy Dispersive X-Ray (EDX) system (EDAX).

Fourier Transform Infrared Spectroscopy (FTIR, FTS 575C, Portman Instruments AG, Software BIO-RAD Win-IR, version 4.14) measurements were conducted on air-dried solids of 28d-reacted HAP from batches conducted at pH 6.5, 7.3 and 9.5 with initial F^- of 3.3, 3.3 and 2.5 mM, respectively (errors for pH 9.5 with 3.3 mM F^- were too high for further consideration of this data). The spectra were compared with those of pure unreacted HAP and FAP and ground mixtures of the two (1 : 3, 1 : 1 and 3 : 1). To differentiate the spectral intensities for the 630 cm^{-1} peak, all data were normalized to the baseline and to unity for the P-O peak at 600 cm^{-1}.

X-Ray Photoelectron Spectroscopy (XPS, Quantum 2000, Physical electronics) was performed on air-dried pure unreacted HAP and FAP, and CaF_2 (rock mineral, AlfaAesar), and on solids obtained from batches conducted at pH 6.5, 7.3 and 9.5 with 7.0, 3.3, and 2.5 mM initial F^-. The XPS analysis employed monochromatic Al Kα radiation and was conducted under constant neutralization using an electron flood gun and very low energy Ar^+ ions (10 eV). Binding energy calibration was carried out

using adventitious carbon, setting the binding energy of C(1s) to 284.8 eV. Spectra were obtained from the untreated surface and after sputter cleaning using an analysis spot with a diameter of 150 μm.

Secondary Ion Mass Spectroscopy (NanoSIMS50, Cameca, Courbevoie, France) was performed on the solid obtained from the batch conducted at pH 6.5 with 7.0 mM initial F^-. Carbon ($^{12}C^-$), fluorine ($^{19}F^-$), phosphorus ($^{31}P^-$), oxygen ($^{16}O^-$) and nitrogen ($^{12}C^{14}N^-$) were detected simultaneously. The analysis was conducted with a lateral dimension of approximately 200 nm x 200 nm and the surface layers were sputtered to a depth of 20 planes corresponding to a maximum depth of 60 - 90 nm.

Experimental set-ups and sample preparations for all solid characterization methods are provided in the Supporting Information (S7-S10).

Results and Discussion

When HAP is (pre)equilibrated in water, the concentrations of Ca^{2+} and PO_4 increase toward their pH-dependent equilibrium values. The presence of these ions in solution will then influence the mechanism(s) by which added F^- is taken up by the solid. Different effects on the solution composition are expected for the various possible mechanisms. In the case of F^- adsorption (mechanism (i)) and / or substitution into the lattice (mechanism (ii)), an increase in the hydroxide (OH^-) concentration, and hence pH, would be expected. If precipitation occurs (mechanism (iii)), decreases in the concentrations of both Ca^{2+} and PO_4, should be observed for FAP precipitation. In the case of CaF_2 precipitation, the PO_4 concentration would be unaffected. Of course, mechanism (iii) can only occur if the prior dissolution of HAP produces sufficiently high concentrations of Ca^{2+} and / or PO_4 that the solutions are supersaturated with respect to a solid phase at a given F^- concentration and pH. In addition to the observed changes in solution composition, evidence for or against the presence of FAP and CaF_2 in the reacted solids was obtained by TEM, FTIR and XPS analyses. The surface enrichment of F^- in the reacted solids was examined by XPS and NanoSIMS.

HAP dissolution as a precondition for fluoride uptake experiments

Dissolution of HAP without pH adjustment (or F^- addition) was observed over 26 d and resulted in an average pH of 7.3 ± 0.1. This equilibrium pH is close to literature values of 7.05[32] and 7.13[33] for the pzc in HAP systems open to the atmosphere. The ionic strength of 2.1 mM was dominated by Ca^{2+}, PO_4, HCO_3^-, K^+ and Cl^-, the latter two diffusing out of the pH electrode. The Ca^{2+} and PO_4 concentrations at 26 d were 0.09 and 0.08 mM respectively, which corresponds to a saturation index of 0.37 ± 0.21 according to the following reaction:

$$Ca_5(PO_4)_3(OH) = 5Ca^{2+} + 3PO_4^{3-} + OH^- \qquad \log K_{s0} = -53.41, 25\ °C^{34}$$

A lower solubility for HAP (log K_{s0} of -58.52) has also been reported.[35]

Uptake of fluoride from aqueous solution

For F^- uptake experiments, HAP suspensions were pre-equilibrated with water for 3 d, allowing the solutions to reach saturation with respect to HAP at pH 7.3 and 9.5. Upon addition of F^-, immediate sharp increases in pH were observed in experiments conducted at pH 6.5 and 7.3, and the pH stat systems required 5 - 15 min to re-adjust the pH to the target values (data not shown). Simultaneous with the pH increases, the F^- concentration decreased. For initial $F^- < 2$ mM at pH 7.3, Ca^{2+} and PO_4 concentrations remained relatively constant, whereas for initial $F^- > 2$ mM, the concentration of Ca^{2+} decreased rapidly and that of PO_4 increased slowly over the 28d-equilibration period (Figure 1a). Calcium and F^- concentrations decreased faster at pH 6.5 than at 7.3 for initial $F^- > 2$ mM (Figure 1a and b). All suspensions at pH 6.5 and those with initial $F^- > 3.3$ mM at pH 7.3 were initially supersaturated with respect to CaF_2 (Table 1) and saturation decreased over 28 d; note that the Ca^{2+} concentration after pre-equilibration was highest at pH 6.5. At pH 9.5, there was an initial increase in pH and concurrent decreases in F^- and Ca^{2+} concentrations were less pronounced, but PO_4 concentrations increased significantly with time (Figure 1a).

Under all conditions, the suspensions were initially supersaturated with respect to FAP. The degree of saturation was lower at pH 6.5 than at pH 9.5 and, in all cases, generally decreased over 28 d. At pH 9.5, the suspensions were also supersaturated with respect to β-tricalciumphosphate (β-TCP, β-$Ca_3(PO_4)_2$). After 28 d, suspensions at pH 9.5 were close to saturation with $CaCO_3$.

The initial sharp pH increases with unchanged Ca^{2+} and PO_4 concentrations in experiments with initial F^- concentrations < 2 mM suggest the exchange of F^- for OH^- ions through adsorption (mechanism (i)) and / or substitution (mechanism (ii)). The adsorption mechanism is consistent with the observation of a plateau in F^- uptake as a function of equilibrium F^- concentration at pH 7.3 after 28 d (Figure 1c). The maximum uptake of 0.009 mmol m^{-2} (0.58 mmol g^{-1}) at pH 7.3 corresponds to 25 % of the initial F^- of 5 mM. The results agree well with those obtained by Bregnhoj,[10] who found a maximum F^- uptake of approximately 0.006 mmol m^{-2} on bone char, in which HAP is the main mineralogical component, after a 3week-equilibration. White et al.[36] found 0.004 mmol m^{-2} F^- uptake on HAP with 1 h equilibration at pH 7.0, 37 °C and 100 mM initial F^-, whereas Lin et al.[22] obtained an uptake capacity of 0.003 mmol m^{-2} on HAP with a reaction time of 2 - 3 h at pH 7.1 - 7.3, 37 °C (initial F^- concentration not reported). In the present study, F^- uptake within 3 h reached ~ 40 % of the maximum uptake for initial F^- < 1 mM and ~ 20 % for initial F^- > 1 mM.

The F^- uptake capacity at pH 6.5 of 0.01 mmol m^{-2} (although based on only three data points) was slightly enhanced relative to that at pH 7.3 (Figure 1c). This trend of higher F^- uptake at lower pH is in agreement with the results of other studies.[22, 37] At pH 9.5, no plateau was observed and the maximum noted F^- uptake was only 0.005 mmol m^{-2}. This is consistent with the observation of fewer available F^- adsorption sites on the HAP / FAP surface at alkaline pH as reported by Bengtsson et al.[16]

220 If the observed uptake of F^- is attributed to the substitution of F^- for OH^- (mechanism (ii)), the corresponding extent of conversion of HAP to FAP would be 33 % at pH 6.5, 30 % at pH 7.3, and 5 %
222 at pH 9.5 (assuming 1.99 mmol OH in 1 g HAP). Since the substitution would be expected to occur first in the unit cells adjacent to the surface, it is useful to estimate how much F^- could be substituted for OH^-
224 given the HAP unit cell dimensions of a = b: 0.91466 nm, c: 0.68745 nm obtained from the XRD reference card.[38] Considering both orientations of a × b and a × c faces of the unit cell toward the
226 solution gives a range of 0.002 to 0.0058 mmol m^{-2} based on exchange of either one or both OH^- within the unit cell. The observed uptake at pH 6.5 (0.01 mmol m^{-2}) and pH 7.3 (0.009 mmol m^{-2}) exceeded the
228 estimated range, which suggests either that both adsorption (mechanism (i)) and substitution of F^- for OH^- (mechanism (ii)) in the first unit cell layer contribute to the observed F^- uptake and / or that F^-
230 diffuses further into the crystal allowing substitution within the bulk. The latter process is likely to be kinetically limited.

232 In the substitution mechanism, FAP is formed by transformation of HAP rather than by HAP dissolution and subsequent FAP precipitation (mechanism (iii)). As previously noted, the PO_4
234 concentration in solution (which derives from the HAP pre-equilibration) did not decrease over 28 d but rather increased. This suggests that FAP is not directly precipitated from solution (mechanism (iii)). If,
236 however, HAP dissolution proceeds throughout the 28d-equilibration, FAP precipitation might limit the accumulation of phosphate in solution thus it may not be possible to exclude this mechanism
238 entirely.[39,40]

At pH 9.5, solutions were also supersaturated with respect to β-TCP (Table 1), but again, it would be
240 expected that its formation would be accompanied by removal of PO_4 from solution, which was not observed. The observed decreases in Ca^{2+} could be related to precipitation of $CaCO_3$, which would in

242 turn decrease the level of saturation with respect to HAP and promote HAP dissolution and the accumulation of PO_4 in solution.

244 Over the course of the 28d-equilibration, unstable solid phases formed as intermediates or, in the case of HAP, present initially would be expected to undergo dissolution in favor of forming FAP as the most 246 thermodynamically stable phase.[26]

Although formation of FAP through (dissolution-)precipitation (mechanism (iii)) seems less likely to 248 control F^- uptake than adsorption and / or substitution (mechanisms (i) and (ii)), the concurrent decrease in Ca^{2+} and F^- at pH 6.5 and 7.3 (with initial $F^- > 2$ mM) is indicative of the precipitation of CaF_2, which 250 is initially oversaturated in these systems. The maximum amount of CaF_2 that could be formed in these systems can be estimated based on the removal of Ca^{2+} from solution to be approximately 4 mg. Diluted 252 into about 2 g of HAP, this amount of CaF_2 would be below the detection limit for XRD analysis (~ 1 - 5 % by mass).

254 **Influence of anions on fluoride uptake**

The anions Cl^-, SO_4^{2-}, and HCO_3^- in excess of F^- (up to 100-fold) had no significant effect on the F^- 256 uptake on HAP during 7d-equilibration (Figure 2). Nor was the uptake affected by the ionic strength (average range: 3 – 350 mM), which is consistent with F^- adsorption on HAP through an inner-sphere 258 binding mechanism.[41]

The relative affinity of HAP for F^- as compared to other ions is likely to be related to the size of the 260 ions (F^-: 0.133 nm; OH^-: 0.137 nm;[20] CO_3^{2-}: 0.178 nm;[42] Cl^-: 0.181 nm;[20] SO_4^{2-}: 0.230 nm[42]) particularly for the substitution mechanism (ii). Substitution of F^- for OH^- would result in the least perturbation of 262 the HAP crystal lattice,[18] while Cl^- and SO_4^{2-} are too large to be easily accommodated. Carbonate is known to substitute into HAP, and this has been found to be associated with release of PO_4 and

decreased stability of the HAP crystal structure.[43] Although this would be expected to decrease F^- uptake, no such effect was observed in this study.

TEM

Transmission micrographs (Figure S1 a-d, Supporting Information) showed typical needle-shaped crystals (dimensions of 50 - 100 nm) for the standard samples of pure, unreacted HAP and FAP, which readily aggregated to form globular particles with dimensions of 1 - 20 μm. The habitus of the crystals remained the same when HAP was equilibrated with F^- at pH 9.5, but at pH 6.5, the equilibrated crystals were generally smaller in size (20 - 80 nm) and appeared irregularly shaped. Similarly-shaped crystals have been observed previously[44] and their habitus attributed to incomplete F^- substitution in HAP. The appearance of the crystals obtained in the present study at pH 6.5 might also reflect partial dissolution of the original HAP.

FTIR

Previous FTIR studies, such as those by Elsami et al.,[45] used the O-H stretching mode at around 3570 cm^{-1} to distinguish qualitatively between HAP and FAP. In the present study, the O-H libration mode at 630 cm^{-1} (which is present in HAP but absent in pure FAP)[46, 47] was used to quantify F^- uptake on HAP. The libration mode corresponds to an infinitely long chain of OH^- ions located in the calcium-phosphate channels of the HAP crystal.[48] This chain decreases in length if F^- substitutes for OH^-, which results in a decrease of the OH-libration intensities.[48] With increased F^- substitution, the libration peak shifts to higher wavenumbers.[48] The appearance of OH^- and F^- related peaks at around 713, 735 and 747 cm^{-1} have been reported for fluoridated HAP samples that were calcined after reaction with F^-,[48, 44] but these were not observed in the present study (Figure S2 a-e, Supporting Information).

The extent of F^- exchange for OH^- was estimated by comparing the FTIR spectra of the pure solids and homogenized mixtures of HAP and FAP (1 : 3, 1 : 1, 3 : 1) with the spectra of solids collected after

28d-equilibration at pH 6.5, 7.3 and 9.5 with initial F^- concentrations of 3.3, 3.3 and 2.5 mM, respectively (Figure 3). On the basis of a linear interpolation of the normalized absorbance at 630 cm^{-1} between pure HAP (0 % F^-), the homogenized HAP-FAP mixtures, and pure FAP (100 % F^-), the extent of substitution of F^- for OH^- is 32 % at pH 6.5, 20 % at pH 7.3 and 2 % at pH 9.5, which is in reasonable agreement with the values calculated based on the uptake of F^- from solution. In addition, slight peak shifts to higher wavenumbers relative to that for HAP were observed with increased F^- uptake (HAP: 628.81 cm^{-1}; pH 9.5: 630.01 cm^{-1}; pH 7.3: 630.01 cm^{-1}, pH 6.5: 630.74 cm^{-1}; Figure 3).

XPS

The surface-sensitive technique of XPS was used to compare the surface composition of the reacted solids with pure unreacted HAP and FAP. Surface sputtering to a depth of approximately 5 nm decreased the average carbon (C) signal from 9.0 ± 2.0 to 3.8 ± 1.6 ($n = 5$) atm % with the C signal assigned mainly to C-C bonds. This signal was thus attributed to surface contamination and therefore carbon was excluded from the compositional analysis presented in Table 2. A surface excess of about 6 atm % was observed for oxygen (O) for both HAP and FAP before sputtering; after sputtering, this surface excess was eliminated for HAP and slightly reduced for FAP. The elemental ratios of Ca / P in the sputtered samples of HAP (1.82) and FAP (1.53) were in reasonable agreement with the nominal value of 1.67.

The data for F abundance in the reacted solids decreased with increasing pH of the equilibration reaction. This trend was observed both before and after sputtering; a slight increase in the F atm % in the sputtered samples likely reflects the removal of some excess O. The %substitution of FAP for HAP in the reacted samples after sputtering were 71 % at pH 6.5, 49 % at pH 7.3 and 22 % at pH 9.5. These values are considerably higher and spread over a more narrow range than those obtained from FTIR and

the changes in solution composition, but may also be influenced by the lower than nominal atm % of Ca and P observed in the XPS (after sputtering) of the reacted solids.

One other key finding from the XPS analysis was that the observed Ca(2p) binding energy in the reacted samples corresponds to that of apatite rather than CaF_2 (Figure S3 a-b, Supporting Information). Since CaF_2 is not infrared active, this solid could not be excluded from the FTIR analysis. The XPS data indicate that F^- is incorporated into the reacted solids in a FAP-like phase, which persists at depths of more than 5 nm into the solid.

NanoSIMS

Additional information on surface composition was obtained using NanoSIMS. While XPS samples a relatively large area (0.02 mm^2), the area sampled by NanoSIMS is much smaller (0.04 μm^2). Thus NanoSIMS has a better chance of sampling individual particles (note that every attempt was made to disperse the particles on the sample holder).

The depth profiles of individual anions ($^{31}P^-$, $^{12}C^-$, and $^{16}O^-$) exhibited maxima at around 18 nm (Figure S4, Supporting Information). This might be related to an increase in the sampled volume with depth (assuming a spherical particle). Since the intensity of the signals reflect the electronegativity of the analytes and provides information only on relative abundance, signals for $^{19}F^-$, $^{12}C^-$, and $^{16}O^-$ were normalized to the signal for $^{31}P^-$ to account for instrumental and matrix effects.

The normalized profile ^{19}F / ^{31}P (Figure 4) of the solid reacted at pH 6.5 with 7.0 mM initial F^- revealed a sharp decrease within the first 6 - 12 nm (3 - 4 ablation planes) corresponding to a decay length (1 / e) of about 4.5 - 6.5 nm. This sharp initial decrease suggests a relative enrichment of fluoride on the sample surface. A similar trend was observed for ^{16}O / ^{31}P with a relatively enrichment of $^{16}O^-$ corresponding to a decay length of 3.8 - 5.7 nm, which probably resulted from sorbed H_2O molecules on the apatite surface. With increased sputtering of the sample, the data become less reliable with

increasing sample depth. In general, the findings are consistent with literature values for a fluoridated surface layer of 3 - 4 nm (neutral pH, 1 h exposure to an undefined concentrated fluoride solution),[22] and of 6 nm (pH 6.2, 5 min exposure to 1.3 mmol NaF).[21] Further, they agree with molecular dynamic models,[23] which suggested a partial F^- incorporation into the HAP crystal.

Comparison of interrogation methods and implications for field applications

Assessment of F^- uptake on HAP through observations of changes in solution chemistry, FTIR and XPS provided reasonably consistent estimates of the uptake capacity of nano-sized HAP. The surface sensitive methods, XPS and NanoSIMS, provided strong evidence for a fluoridated surface layer though NanoSIMS showed a decrease in F^- abundance with depth that was not evident in XPS. It is, however, likely that XPS, since it samples a larger area, averages a signal over more particles than NanoSIMS.

The analytical approaches used could not distinguish unambiguously among the possible F^- uptake mechanisms of adsorption, substitution and (dissolution-)precipitation, but suggest the presence of FAP-like phases in all reacted solid products. The evolution of the PO_4 concentrations in solutions equilibrated with HAP and F^- do not support the (dissolution-)precipitation mechanism but cannot entirely exclude it. The changes in solution chemistry do indicate that CaF_2 is precipitated initially, but the XPS results indicate that any precipitated CaF_2 is replaced by FAP over the 28d-equilibration.

In the experimental systems studies here, HAP was equilibrated with F^- over 28 d. This long equilibration time is not representative of how HAP-based filters would be deployed in the field. Shorter equilibration times would tend to limit the accumulation of Ca^{2+} and PO_4 (i.e., by HAP dissolution) in the pore spaces of the filter. The adsorption mechanism would be more likely to predominate under these conditions and, in the case of alkaline water, F^- uptake might be very low. This could be offset by pH adjustment to increase F^- uptake, but this may be logistically difficult in developing countries. Another option would be to mix a relatively soluble Ca- and PO_4-containing

mineral into the filter material. This would provide ions for precipitation reactions and thus enhance the
356 F^- uptake capacity on HAP-based filters.

Acknowledgements

358 We thank Stephan Hug for valuable discussions on FTIR analysis and Hermann Moench for the assistance and advice in various laboratory works. The author VS thanks Claire Farnsworth for fruitful
360 discussions. Also, two anonymous reviewers (R1 and R2) are acknowledged for their constructive feedback. We acknowledge funding from the Swiss National Science Foundation (200021-117992).

362 **Supporting Information Available**

The supporting information provides details of the solid characterization of HAP, synthesis of FAP,
364 methods of fluoride, cation and anion measurements, and analysis of total dissolved carbon, as well as details of XRD, TEM, FTIR, XPS, and NanoSIMS analyses of the solid products. This information is
366 available free of charge via the Internet at http://pubs.acs.org/.

References

368 (1) Fawell, J.; Bailey, K.; Chilton, J.; Dahi, E.; Fewtrell, L.; Magara, Y. Fluoride in Drinking-water. WHO, 2001, http://www.who.int/water_sanitation_health/publications/fluoride_drinking_water/en/.

370 (2) Hodge, H. C. The concentration of fluorides in drinking water to give the point of minimum caries with maximum safety. *J. Am. Dent. Assoc.* **1950,** *40;* 436-439.

372 (3) Nair, K. R.; Manji, F. *The occurrence and distribution of fluoride in groundwaters of Kenya*, Challenges in African Hydrology and Water Resources: Proceedings of the Harare Symposium, Harare,
374 Zimbabwe, 1984.

(4) Reimann, C.; Bjorvatn, K.; Frengstad, B.; Melaku, Z.; Tekle-Haimanot, R.; Siewers, U. Drinking
376 water quality in the Ethiopian section of the East African Rift Valley I--data and health aspects. *Sci. Total Environ.* **2003,** *311* (1-3); 65-80, DOI: 10.1016/S0048-9697(03)00137-2.

378 (5) Teotia, S. P. S.; Teotia, M.; Singh, R. K. Hydro-Geochemical Aspects of Endemic Skeletal Fluorosis in India - an Epidemiologic Study. *Fluoride.* **1981,** *14* (2); 69-74.

380 (6) Bo, Z.; Mei, H.; Yongsheng, Z.; Xueyu, L.; Xuelin, Z.; Jun, D. Distribution and Risk Assessment of Fluoride in Drinking Water in the West Plain Region of Jilin Province, China. *Environ. Geochem. Health.* **2003,** *25* (4); 421-431, DOI: 10.1023/B:EGAH.0000004560.47697.91.

384 (7) Diaz-Barriga, F.; Navarro-Quezada, A.; Grijalva, M. I.; Grimaldo, M.; Loyola-Rodriguez, J. P.; Deogracias Ortiz, M. Endemic fluorosis in Mexico. *Fluoride.* **1997,** *30* (4); 233-239.

(8) Paoloni, J. D.; Fiorentino, C. E.; Sequeira, M. E. Fluoride contamination of aquifers in the southeast subhumid pampa, Argentina. *Environ. Toxicol.* **2003,** *18* (5); 317-320, DOI: 10.1002/tox.10131.

(9) Dorozhkin, S. V.; Epple, M. Biological and Medical Significance of Calcium Phosphates. *Angew. Chem. Int. Edit.* **2002,** *41* (17); 3130-3146.

(10) Bregnhoj, H. Processes and Kinetics of Defluoridation of Drinking Water Using Bone Char. Ph.D. Dissertation, Technical University of Denmark, Lyngby, 1995.

(11) Larsen, M. J.; Pearce, E. I. F.; Jensen, S. J. Defluoridation of Water at High pH with Use of Brushite, Calcium Hydroxide, and Bone Char. *J. Dent. Res.* **1993,** *72;* 1519-1525.

(12) HealthCanada Guidelines for Canadian Drinking Water Quality: Guideline Technical Document - Fluoride. Water, A. a. C. C., Ottawa, 2010 http://www.hc-sc.gc.ca/ewh-semt/alt_formats/hecs-sesc/pdf/pubs/water-eau/2011-fluoride-fluorure/2011-fluoride-fluorure-eng.pdf.

(13) Dahi, E. *Contact precipitation for defluoridation of water*, 22nd WEDC Conference: Reaching the unreached: Challenges for the 21st century, New Delhi, India, 1996.

(14) Elliott, J. *Structure and Chemistry of the Apatites and Other Calcium Orthophosphates*, in Studies in Inorganic Chemistry, 18; Elsevier Science: Amsterdamm, Netherlands, 1994.

(15) Gaines, R. V.; Skinner, H. C. W.; Foord, E. E.; Mason, B.; Rosenzweig, A. *Dana's New Mineralogy*, 8, ed.; John Wiley & Sons, Inc.: New York, NY, 1997.

(16) Bengtsson, Å.; Shchukarev, A.; Persson, P.; Sjöberg, S. Phase Transformations, Ion-Exchange, Adsorption, and Dissolution Processes in Aquatic Fluorapatite Systems. *Langmuir* **2009,** *25* (4); 2355-2362, DOI: 10.1021/la803137u.

(17) McCann, H. G. Reactions of fluoride ion with hydroxyapatite. *J. Biol. Chem.* **1953,** *201* (1); 247-259.

(18) Aoba, T. The effect of fluoride on apatite structure and growth. *Crit. Rev. Oral Biol. Med.* **1997,** *8* (2); 136-153.

(19) Kohn, M. J.; Rakovan, J.; Hughes, J. M. *Phosphates: geochemical, geobiological and material importance. Reviews in Mineralogy and Geochemistry*, MSA: Washington, DC, 2002.

(20) Shannon, R. D. Revised effective ionic radii and systematic studies of interatomic distances in halides and chalcogenides. *Acta Cryst.* **1976,** *32* (5); 751-767.

(21) Mueller, F.; Zeitz, C.; Mantz, H.; Ehses, K.-H.; Soldera, F.; Schmauch, J.; Hannig, M.; Huefner, S.; Jacobs, K. Elemental Depth Profiling of Fluoridated Hydroxyapatite: Saving Your Dentition by the Skin of Your Teeth? *Langmuir* **2010,** *26* (24); 18750-18759, DOI: 10.1021/la102325e.

(22) Lin, J.; Raghavan, S.; Fuerstenau, D. W. The adsorption of fluoride ions by hydroxyapatite from aqueous solution. *Colloid. Surface.* **1981,** *3* (4); 357-370, DOI 10.1016/0166-6622(81)80062-5.

(23) de Leeuw, N. H. Resisting the Onset of Hydroxyapatite Dissolution through the Incorporation of Fluoride. *J. Phys. Chem.* **2004,** *108* (6); 1809-1811, DOI: 10.1021/jp036784v.

(24) Christoffersen, J.; Christoffersen, M. R.; Arends, J.; Leonardsen, E. S. Formation of phosphate-containing calcium fluoride at the expense of enamel, hydroxyapatite and fluorapatite. *Caries Res.* **1995,** *29* (3); 223-230.

(25) Spinelli, M. A.; Brudevold, F.; Moreno, E. Mechanism of fluoride uptake by hydroxyapatite. *Arch. Oral Biol.* **1971,** *16;* 187-203.

(26) Stumm, W.; Morgan, J. J. *Aquatic Chemistry: Chemical Equilibria and Rates in Natural Waters*, 3, ed.; John Wiley & Sons, Inc.: Hoboken, NJ, 1996.

(27) Gao, S.; Sun, R.; Wei, Z.; Zhao, H.; Li, H.; Hu, F. Size-dependent defluoridation properties of synthetic hydroxyapatite. *J. Fluorine Chem.* **2009,** *130* (6); 550-556, DOI: 10.1016/j.jfluchem.2009.03.007.

(28) Ramsey, A. C.; Duff, E. J.; Paterson, L.; Stuart, J. L. The Uptake of F- by Hydroxyapatite at Varying pH. *Caries Res*. **1973,** *7* (3); 231-244, DOI: 10.1159/000259846.

(29) Fan, X.; Parker, D. J.; Smith, M. D. Adsorption kinetics of fluoride on low cost materials. *Water Res*. **2003,** *37* (20); 4929-4937.

(30) Sundaram, C. S.; Viswanathan, N.; Meenakshi, S. Defluoridation chemistry of synthetic hydroxyapatite at nano scale: Equilibrium and kinetic studies. *J. Hazard. Mater*. **2008,** *155* (1-2); 206-215, DOI: 10.1016/j.jhazmat.2007.11.048.

(31) Hammari, L. E. L.; Laghzizil, A.; Barboux, P.; Lahlil, K.; Saoiabi, A. Retention of fluoride ions from aqueous solution using porous hydroxyapatite: Structure and conduction properties. *J. Hazard. Mater*. **2004,** *114* (1-3); 41-44, DOI: 10.1016/j.jhazmat.2004.06.032.

(32) Attia, Y. A.; Fuerstenau, D. W. The equilibrium composition of hydroxyapatite and fluorapatite-water interfaces. *Colloid. Surface*. **1988,** *34* (3); 271-285, DOI: 10.1016/0166-6622(88)80105-7.

(33) Wu, L.; Forsling, W.; Schindler, P. W. Surface complexation of calcium minerals in aqueous solution : 1. Surface protonation at fluorapatite-water interfaces. *J. Colloid Interface Sci*. **1991,** *147* (1); 178-185, DOI: 10.1016/0021-9797(91)90145-X.

(34) Zhu, Y.; Zhang, X.; Chen, Y.; Xie, Q.; Lan, J.; Qian, M.; He, N. A comparative study on the dissolution and solubility of hydroxyapatite and fluorapatite at 25°C and 45°C. *Chem. Geol*. **2009,** *268* (1-2); 89-96, DOI: 10.1016/j.chemgeo.2009.07.014.

(35) McDowell, H.; Gregory, T. M.; Brown, W. E. Solubility of Ca5(P04)3OH in the System Ca(OH)2-H3P04-H20 at 5, 15, 25, and 37 °C *J. Res. Nat. Bur. Stand*. **1977,** *81A;* 273-281.

(36) White, D. J.; Bowman, W. D.; Faller, R. V.; Mobley, M. J.; Wolfgang, R. A.; Yesinowski, J. P. 19F MAS-NMR and solution chemical characterization of the reactions of fluoride with hydroxyapatite and powdered enamel. *Acta. Odontol. Scand*. **1988,** *46* (6); 375-389.

(37) Nelson, K.; Higuchi, W. I. Mechanism of fluoride uptake by hydroxyapatite from acidic fluoride solutions: I. Theoretical considerations. *J. Dent. Res*. **1970,** *49* (6); 1541-1548.

(38) Hughes, J. M.; Cameron, M.; Crowley, K. D. Structural variations in natural F, OH, and Cl apatites. *Am Mineral* **1989,** *74* (7-8); 870-876.

(39) Pasteris, J. D.; Ding, D. Y. Experimental fluoridation of nanocrystalline apatite. *Am Mineral* **2009,** *94* (1); 53-63, DOI: 10.2138/am.2009.2926.

(40) Putnis, A. Mineral replacement reactions: from macroscopic observations to microscopic mechanisms. *Mineral Mag* **2002,** *66* (5); 689-708, DOI: 10.1180/0026461026650056.

(41) Stumm, W. *Chemistry of the solid-water interface: Processes at the mineral-water and particle-water interface in natural systems*, John Wiley & Sons, Inc.: New York, NY, 1992.

(42) Marcus, Y. *Ion properties*, Marcel Dekker Inc.: New York, NY, 1997.

(43) Shellis, R. P.; Lee, A. R.; Wilson, R. M. Observations on the Apparent Solubility of Carbonate-Apatites. *J. Colloid Interface Sci*. **1999,** *218* (2); 351-358.

(44) Rodriguez-Lorenzo, L. M.; Hart, J. N.; Gross, K. A. Influence of fluorine in the synthesis of apatites. Synthesis of solid solutions of hydroxy-fluorapatite. *Biomaterials* **2003,** *24* (21); 3777-3785, DOI: 10.1016/S0142-9612(03)00259-X.

(45) Eslami, H.; Solati-Hashjin, M.; Tahriri, M. The comparison of powder characteristics and physicochemical, mechanical and biological properties between nanostructure ceramics of hydroxyapatite and fluoridated hydroxyapatite. *Mater. Sci. Eng. C*. **2009,** *29* (4); 1387-1398, DOI: 10.1016/j.msec.2008.10.033.

(46) Fowler, B. O. Infrared studies of apatites. I. Vibrational assignments for calcium, strontium, and barium hydroxyapatites utilizing isotopic substitution. *Inorg. Chem*. **1974,** *13* (1); 194-207.

(47) Rintoul, L.; Wentrup-Byrne, E.; Suzuki, S.; Grondahl, L. FT-IR spectroscopy of fluoro-substituted hydroxyapatite: strengths and limitations. *J. Mater. Sci. Mater. Med.* **2007,** *18* (9); 1701-1709, DOI: 10.1007/s10856-007-3052-3.

(48) Freund, F.; Knobel, R. M. Distribution of fluorine in hydroxyapatite studied by infrared spectroscopy. *J Chem Soc Dalton* **1977,** (11); 1136-1140, DOI: 10.1039/DT9770001136.

(49) Martell, A. E.; Smith, R. M. *Critical stability constants*, Plenum Press: New York, NY, 1974-1989.

(50) Woods, T. L.; Garrels, R. M. *Thermodynamic values at low temperature for natural inorganic materials: An uncritical summary* Oxford University Press: New York, NY, 1987.

(51) Cammann, K.; Galster, H. *Das Arbeiten mit ionenselektiven Elektronen: Eine Einfuehrung fuer Praktiker*, 3, ed.; Springer: Berlin, Germany, 1996.

(52) El Feki, H.; Rey, C.; Vignoles, M. Carbonate ions in apatites: Infrared investigations in the v4 CO3 domain. *Calcif Tissue Int* **1991,** *49* (4); 269-274.

(53) Elliott, J.; Holcomb, D.; Young, R. Infrared determination of the degree of substitution of hydroxyl by carbonate ions in human dental enamel. *Calcif Tissue Int* **1985,** *37* (4); 372-375.

TABLE 1. Concentrations of F^-, Ca^{2+} and PO_4 and saturation indices for relevant solids for batches conducted at pH 6.5, 7.3 and 9.5 with initial F^- of 2.5 - 7.0 mM, a) after 3d-pre-equilibration before F^- addition (potential saturation indices for CaF_2 and FAP), and b) after 20 - 28 d equilibration in F^- solution.

Sample		F_{tot} [mM]	Ca_{tot} [mM]	$PO_{4\,tot}$ [mM]	Saturation Index			
					HAP	CaF_2	FAP	β-TCP
pH6.5	a		0.13±0.01	0.21±0.06	-5.61±-5.67	**0.88**±0.08	**2.16**±2.11	-4.10±-4.32
3.3mM	b	1.67±0.05	0.02±0.01	0.19±0.004	-9.84±-9.86	-0.60±-0.93	-2.40±-2.43	-6.71±-6.80
pH6.5	a		0.34±0.005	0.20±0.01	-2.35±-3.48	**2.11**±0.57	**5.79**±4.77	-2.06±-3.32
7.0mM	b	5.09±0.20	0.03±0.02	0.24±0.02	-8.53±-8.16	**0.56**±0.41	-0.51±-0.14	-6.03±-5.77
pH7.3	a		0.21±0.06	0.12±0.03	**0.08**±-0.44	**1.08**±0.56	**7.04**±6.52	-0.88±-1.41
3.3mM	b	2.29±0.11	0.01±0.01	0.16±0.01	-5.63±-5.53	-0.46±-0.81	**1.12**±1.22	-4.45±-4.43
pH9.5	a		0.01±0.001	0.13±0.01	**2.39**±2.22	-0.67±-1.40	**7.07**±6.89	-0.29±-0.68
2.5mM	b	2.23±0.09	0.03±0.01	0.28±0.02	**5.67**±5.72	-0.07±-0.53	**10.27**±10.33	**1.56**±1.48

Saturation indices were calculated according to $S = \log\left(\frac{IAP}{K_{s0}}\right)^{\frac{1}{\eta}}$, where IAP is the ion activity product, K_{s0} is the solubility product and η is the number of ions in the formula unit of the considered mineral.[41] The IAP was adjusted for each individual sample; K_{s0} was corrected according to Davies for the individual activity coefficients. Hydroxyapatite (HAP): $5Ca^{2+} + 3PO_4^{3-} + OH^-$; log K_{s0HAP} = -53.28;[34] fluorite (CaF_2): $Ca^{2+} + 2F^-$; log Ks_{0CaF2} = -10.50;[49] fluorapatite (FAP): $5Ca^{2+} + 3PO_4^{3-} + F^-$; log K_{s0FAP} = -56.12;[34] β-tricalciumphosphate (β-TCP): $3Ca^{2+} + 2PO_4^{3-}$; log K_{s0TCP} = -28.92.[50] Bold numbers indicate saturation of the specific phase; (-) DIC not measured.

TABLE 2. Surface composition of pure unreacted HAP and FAP, CaF_2 and of solids collected from batches conducted at pH 6.5, 7.3 and 9.5 with 7.0, 3.3, 2.5 mM initial F^-, respectively [atm %] obtained from XPS analysis. Upper section: nominal values. Middle section: values obtained before sputtering. Lower section: values obtained after sputtering.

	O(1s)	F(1s)	P(2p)	Ca(2p)	Ca/P	Ca/F	O/P	F/O	F/P
HAP (nominal)	61.9	0.0	14.3	23.8	1.67	-	4.4	-	-
FAP (nominal)	57.1	4.8	14.3	23.8	1.67	4.8	4.1	0.087	0.4
CaF_2 (nominal)	0.0	66.7	0.0	33.3	-	0.5	-	-	-
before sputtering									
HAP	65.7	0.0	14.1	20.2	1.43	-	4.7	-	-
FAP	60.8	4.0	14.2	21.0	1.47	5.2	4.3	0.066	0.3
CaF_2	0.0	63.7	0.0	36.3	-	0.6	-	-	-
pH6.5-7.0	61.7	3.0	14.1	21.3	1.51	7.2	4.4	0.048	0.2
pH7.3-3.3	62.8	2.3	14.2	20.7	1.46	9.1	4.4	0.036	0.2
pH9.5-2.5	64.7	1.2	13.4	20.8	1.55	17.6	4.8	0.018	0.1
after sputtering									
HAP	61.8	0.0	13.5	24.5	1.82	-	4.6	-	-
FAP	59.8	4.5	14.1	21.5	1.53	4.8	4.2	0.075	0.3
CaF_2	0.0	64.8	0.0	35.1	-	0.5	-	-	-
pH6.5-7.0	59.0	3.6	13.7	23.8	1.73	6.7	4.3	0.060	0.3
pH7.3-3.3	60.6	2.4	13.7	23.2	1.69	9.5	4.4	0.040	0.2
pH9.5-2.5	63.2	1.1	13.6	22.2	1.63	20.0	4.7	0.018	0.1

Figure captions

514 **FIGURE 1. (a) Total dissolved Ca^{2+} concentrations at pH 6.5 (□), 7.3 (□), and 9.5 (Δ), and PO_4 concentrations (filled symbols) from batches with 3.3 mM initial F^- at 25 °C and [HAP] = 2 g L^{-1}.**

516 **(b) Total dissolved F^- concentration. (c) Fluoride uptake (mmol m^{-2}) on HAP. Error bars present the standard deviation (n = 2) and are sometimes smaller than the symbols.**

518 **FIGURE 2. Average F^- uptake (n = 2) obtained in HAP suspensions [2 g L^{-1}] with 0.5 mM initial F^- at pH 7.3 and 25 °C: red: sulphate (0.5 ± 0.05, 5 ± 0.5, and 50 ± 5 mM); green: chloride**

520 **(0.5 ± 0.05, 5 ± 0.5, and 50 ± 5 mM); and blue: bicarbonate (5 ± 0.2 and 50 ± 12 mM). Error bars present the standard deviation; solid lines present F^- uptake ± standard deviation without any**

522 **anion addition. The average background electrolyte composition had an ionic strength of 3 - 350 mM as a result of pH adjustment (as $NaNO_3$), dissolution of HAP and addition of sodium**

524 **salts, including NaF.**

FIGURE 3. FTIR absorbance spectra for the following phases: 100 % HAP (black),

526 **3 HAP : 1 FAP (dark grey), 1 HAP : 1 FAP (medium grey), 1 HAP : 3 FAP (light grey), 100 % FAP (pale grey), solids from batch pH 6.5 (red), pH 7.3 (green), and pH 9.5 (blue) with initial F^- of**

528 **3.3, 3.3 and 2.5 mM, respectively. The data shown were normalized to the baseline and to 1.0 for the P-O peak at 600 cm^{-1}.**

530 **FIGURE 4. NanoSIMS measurements of the ratios ^{19}F / ^{31}P (thick solid line, scale on the left y-axis), ^{12}C / ^{31}P (dotted line, scale on the left y-axis) and ^{16}O / ^{31}P (thin solid line, scale on the right**

532 **y-axis). The analyzed solids were collected from the batch at pH 6.5 with 7.0 mM initial F^-.**

FIGURE 1.

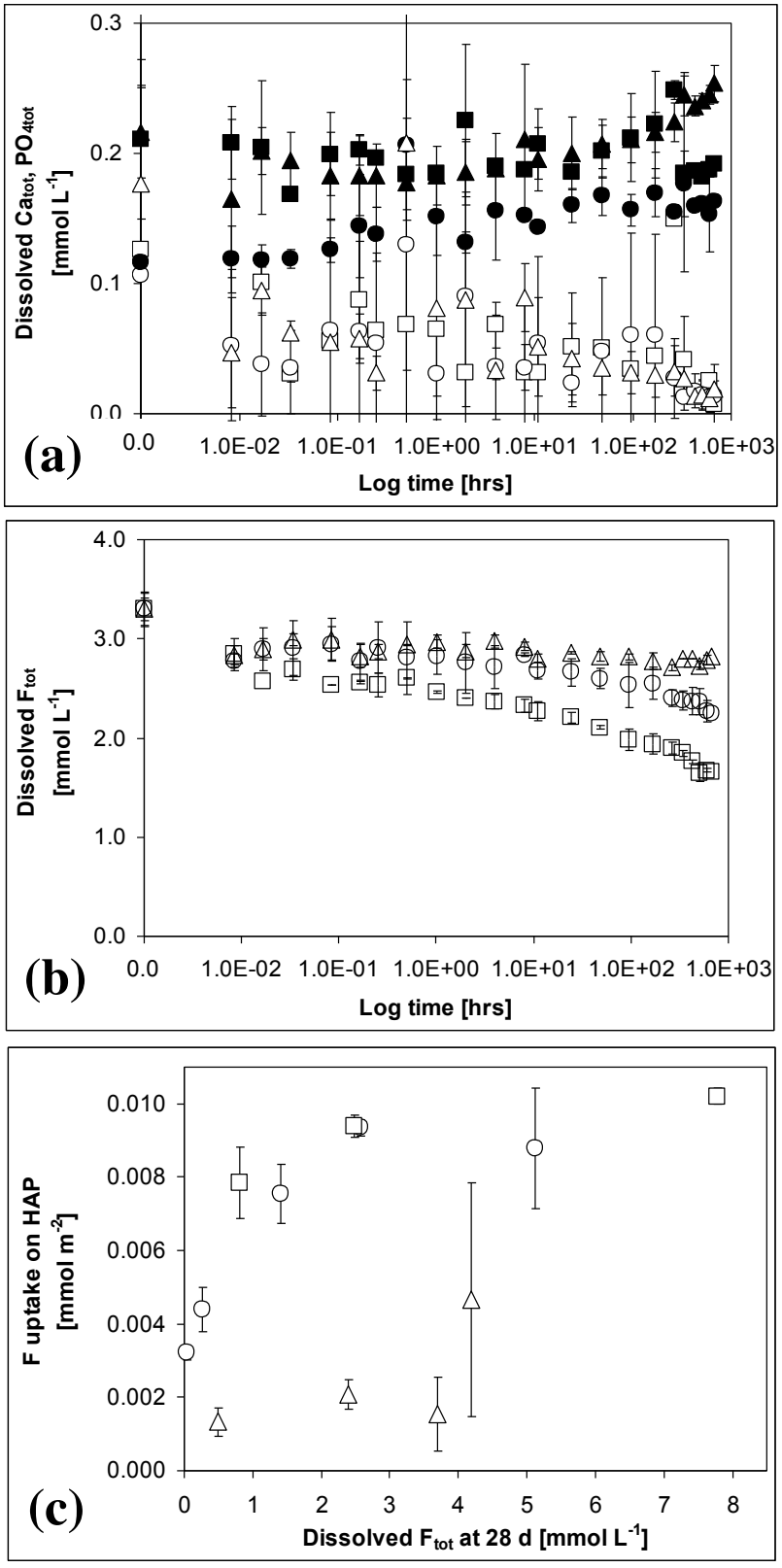
0.3
0.2
0.1
0.0
Dissolved Catot, PO4tot [mmol L-1]
(a)
0.0
1.0E-02
1.0E-01
1.0E+00
1.0E+01
1.0E+02
1.0E+03
Log time [hrs]
4.0
3.0
2.0
1.0
0.0
Dissolved Ftot [mmol L-1]
(b)
0.0
1.0E-02
1.0E-01
1.0E+00
1.0E+01
1.0E+02
1.0E+03
Log time [hrs]
0.010
0.008
0.006
0.004
0.002
0.000
F uptake on HAP [mmol m-2]
(c)
0
1
2
3
4
5
6
7
8
Dissolved Ftot at 28 d [mmol L-1]

FIGURE 2.

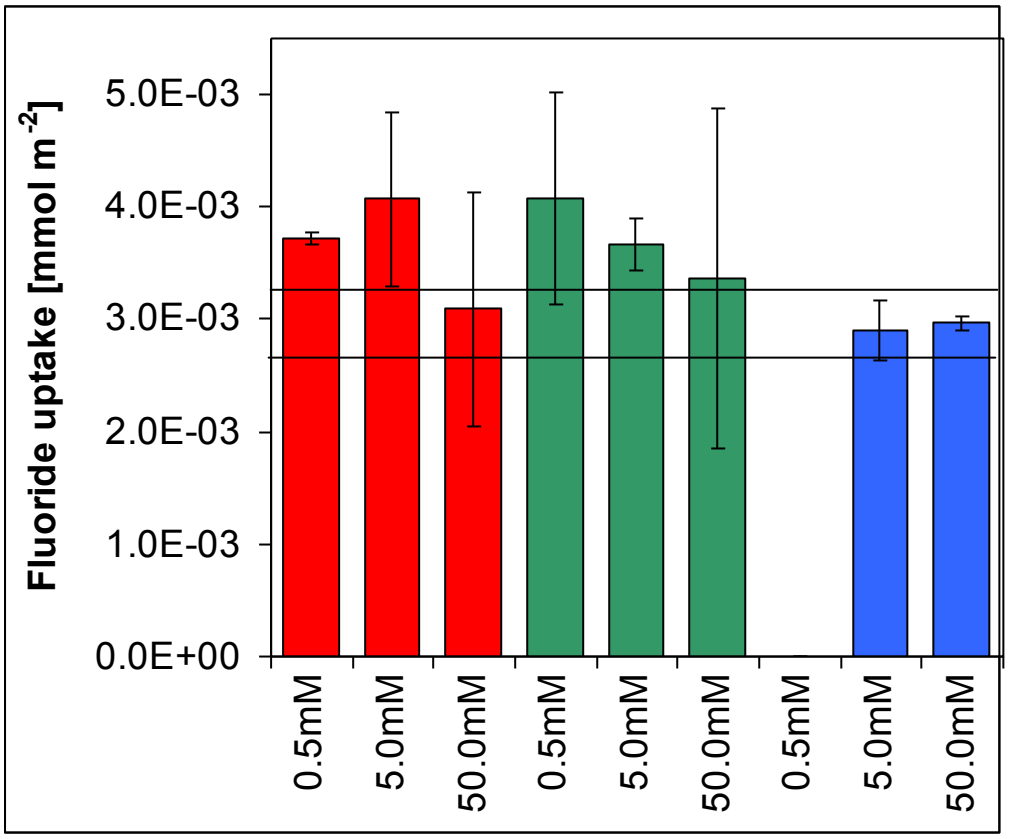
Fluoride uptake [mmol m-2]
5.0E-03
4.0E-03
3.0E-03
2.0E-03
1.0E-03
0.0E+00
0.5mM
5.0mM
50.0mM
0.5mM
5.0mM
50.0mM
0.5mM
5.0mM
50.0mM

588

FIGURE 3.

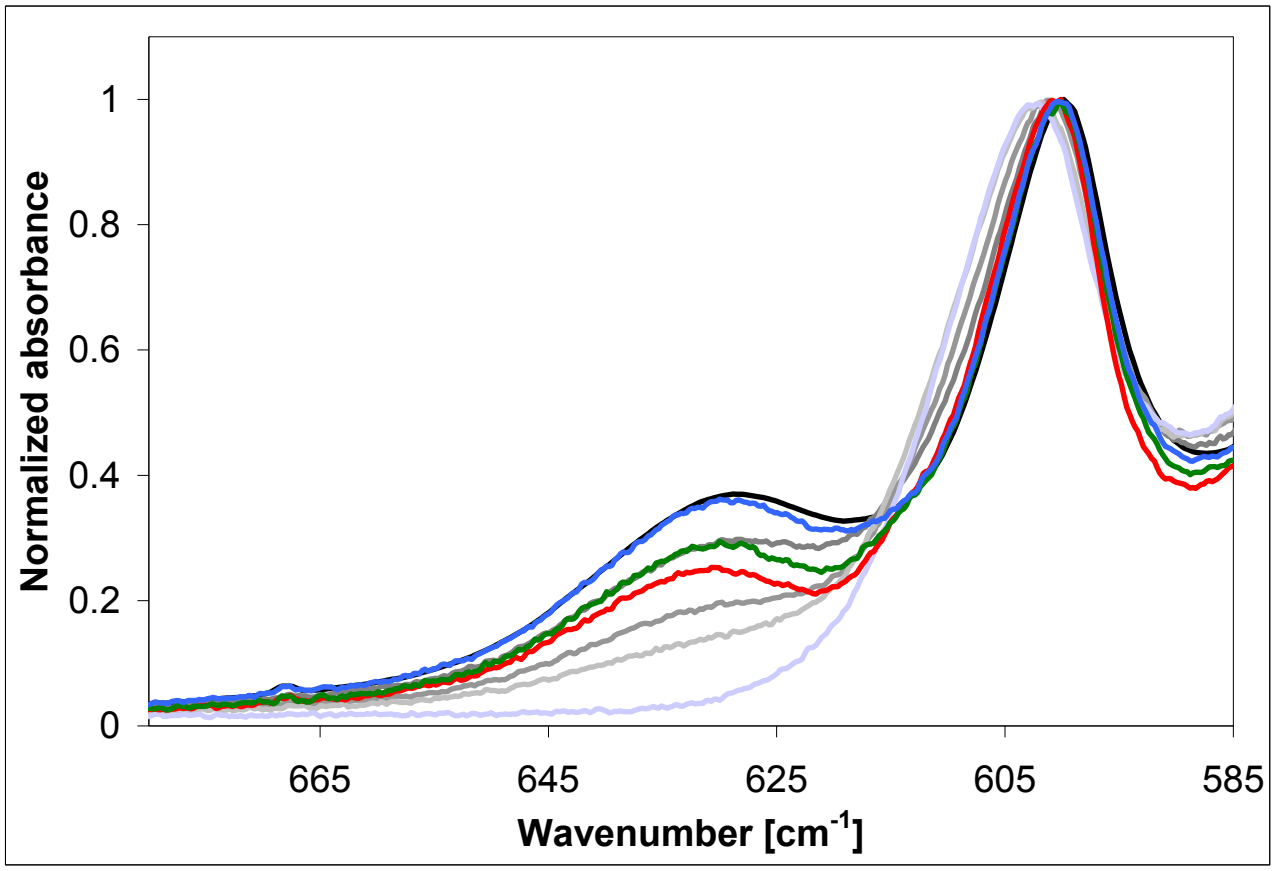

590

592 **FIGURE 4.**

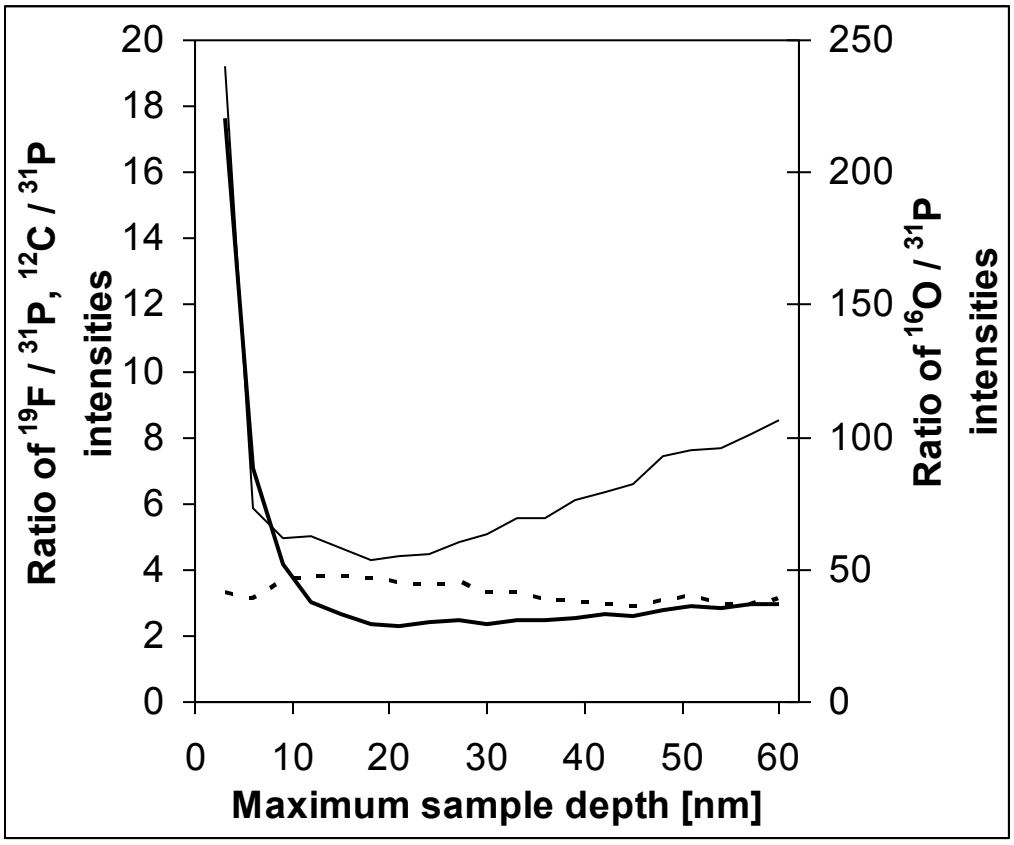

594